Inorganic Chemistry Research

Article

# Nano-Ferrite $ZnFe_2O_4$ as Efficient and Re-Usable Catalyst for the Synthesis of 4*H*-Chromenes and 4*H*-Pyrano[2,3-c] pyrazoles

Razieh Nejat*

*Chemistry Department, Faculty of Science, Kosar University of Bojnord, Iran. Bojnord, Iran. P.O. Box 9415615458*

Received: September 15, 2021; Accepted: December 24, 2021

**Cite This:** *Inorg. Chem. Res.* **2022**, *6*, 10-16. DOI: 10.22036/icr.2021.304989.1118

**Abstract**: Nano-magnetic ferrite $ZnFe_2O_4$ among other magnetic nanoparticles include $Fe_2O_3$, $Fe_3O_4$, $Ni_{(0.7)}Zn_{(0.3)}Fe_2O_4$ and $Mn_{(0.7)}Zn_{(0.3)}Fe_2O_4$ was explored as an efficient catalyst for the synthesis of various 4H-Chromenes and 4H-Pyrano[2,3-c]pyrazoles in EtOH/$H_2O$ (2:1) via an easy and green procedure. The desired products were obtained in high yields via a three-component reaction between aromatic aldehydes with malononitrile and 5,5-dimethyl-cyclohexane-1,3-dione or 3-methyl-1-phenyl-2-pyrazolin-5-one at room temperature. The structure of this catalyst was fully characterized via Fourier transform infrared spectroscopy, XRD, SEM, TEM, EDAX, and VSM. The employed nanocatalyst was easily recovered using a magnetic field and reused ten times (in subsequent runs) without observation a significant decrease in activity.

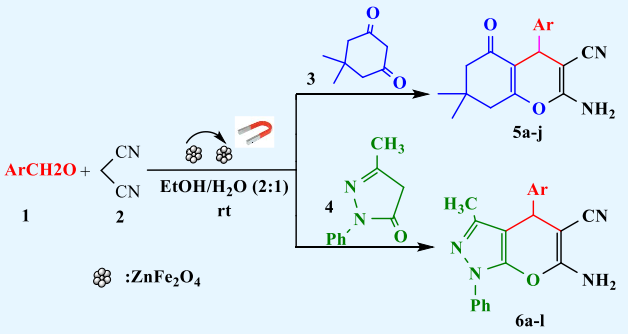


**Keywords:** Nano-magnetic ferrite, Chromenes, pyrazoles, $ZnFe_2O_4$

## 1. INTRODUCTION

Metal nano-oxides have been well-documented during the last few years as versatile heterogeneous catalysts in various organic transformations owing to their high ratios of surface area to volume.[1,2] Among these, magnetic metal nanoparticles have been the focus of much research interests for their unique properties and potential applications such as catalytic activities for epoxidation,[3] benzylation,[4] drug delivery, as magnetic resonance imaging (MRI) contrast agents, hypothermia, and magnetic separation of biomolecules.[5,6] Moreover, the magnetic property of these catalysts enables them to be completely separated simply by means of an external magnetic field and re-used without considerable loss of their catalytic activities.[7-21]

Since the spinel ferrites crystallize in a face-centered cubic (FCC) lattice containing eight formula units in the cubic unit cell, they can be distinguished as two basic types, i.e. normal and inverse spinels.[22] The composition of the spinel ferrites can be described by the general formula $M^{2+}[Fe^{3+}Fe^{3+}]O_4$ which exhibits applications in both technological and catalytical fields.[23] In spinel ferrites, the oxygen anions from an FCC lattice, and the cations occupy the interstitial positions. There are two interstitial sites, one is tetrahedral (T) surrounded by four oxygen anions and the other is octahedral (O) surrounded by six oxygen anions. In the spinel ferrites of the formula $MFe_2O_4$, the metal cations $M^{2+}$ and $Fe^{3+}$ can occupy both the octahedral and tetrahedral sites. The spinel lattice will be a normal spinel when the $M^{2+}$ cations occupy the tetrahedral sublattices in the cubic closed-packed $O^{2-}$ lattice, otherwise, the ferrite will be of an inverse spinel-type. If both of the sublattices contain $M^{2+}$ and $Fe^{3+}$ cations, the ferrite will exist as mixed spinel. Occupations by the cations at these sites have an important effect on the properties of the spinels including the magnetic behavior, conductivity and catalytic activity.[24-26]

Zinc ferrites have normal spinel structures, whereas $Fe_3O_4$ has an inverse spinel structure in which all the $Fe^{2+}$ ions occupy half of the octahedral sites and the $Fe^{3+}$ ions are split evenly across the remaining octahedral and tetrahedral sites. Both the Ni/Zn and Mn/Zn ferrites have mixed spinel structure with the unit cell consisting eight units of the forms $[Zn_x^{2+}Fe_{1-x}^{3+}]_{tet}[Ni_{1-x}^{2+}Fe_{1+x}^{3+}]_{oct}O_4^{2-}$ and $[Zn_x^{2+}Fe_{1-x}^{3+}]_{tet}[Mn_{1-x}^{2+}Fe_{1+x}^{3+}]_{oct}O_4^{2-}$. The $Zn^{2+}$ cations preferably occupy the tetrahedral sites, whereas the $Ni^{2+}$ and $Mn^{2+}$ cations always occupy the octahedral sites.[27, 28]

In addition, the growing number of reports throughout the literature reveals the importance of one-pot multicomponent reactions (MCRs) as a useful strategy in synthetic organic and bioorganic chemistry.[29-31] Moreover, the synthesis of 4*H*-chromene derivatives

constitutes an important class of heterocyclic compounds which are present in a number of biologically and pharmacologically active products.[32-34] In addition, the fused pyrazolones including pyrano derivatives represent another important class of heterocyclic compounds since they exhibit vital biological and pharmacological properties. Recently, several methods appeared describing the facile synthesis of these heterocycles.[35-40]

## 3. RESULTS AND DISCUSSION

As part of our current studies on the development of new and efficient approaches to the synthesis of biologically important heterocyclic compounds,[41-44] herein, we describe a three-component synthesis of highly functionalized 4*H*-chromenes and 4*H*-pyrano[2,3-c]pyrazoles. Thus, a mixture of aromatic aldehyde (**1**), malononitrile (**2**), and 5,5-dimethylcyclohexane-1,3-dione (dimedone) (**3**) or 3-methyl-1-phenyl-2-pyrazolin-5-one (**4**) under the catalytic effect of various magnetic oxide nanoparticles such as $Fe_2O_3$, $Fe_3O_4$, $ZnFe_2O_4$, $Ni_{0.7}Zn_{0.3}Fe_2O_4$ and $Mn_{0.7}Zn_{0.3}Fe_2O_4$ undergo one-pot reactions in EtOH/$H_2O$ (2:1) at room temperature to afford the corresponding 4*H*-chromenes **5** and 4*H*-pyrano[2,3-c]pyrazoles (**6**) respectively (Scheme 1).

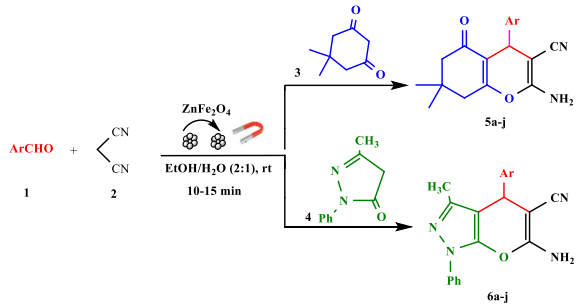


**Scheme 1.** Schematic representation of the synthesis of 4*H*-chromenes **5** and 4*H*-pyrano[2,3-c]pyrazoles **6** in the present of $ZnFe_2O_4$ as catalyst

To establish the reaction conditions, we initially studied the reaction between benzaldehyde, malononitrile and dimedone as the model reaction. The effects of the catalyst and solvent on the reaction were investigated using different magnetic oxide nanoparticles such as $Fe_2O_3$, $Fe_3O_4$, $ZnFe_2O_4$, $Ni_{0.7}Zn_{0.3}Fe_2O_4$ and $Mn_{0.7}Zn_{0.3}Fe_2O_4$ under various catalytic loadings in different solvents including $H_2O$, EtOH, $CH_3CN$ (Table 1). As shown in Table 1, the reaction worked out best in terms of the reaction time (10 min), and the yield (90%) in the presence of zinc ferrite ($ZnFe_2O_4$) nanoparticles (5 mol%) in the mixed EtOH/$H_2O$ (2:1) as the solvent of choice at room temperature (entry 5).

The results in Figure 1 suggest that among the catalysts examined in this reaction, the nano-zinc ferrite $ZnFe_2O_4$ appears as the most effective catalyst. After completion of the reaction, hot absolute ethanol was added and the catalyst was absorbed on the magnetic stirring bar. The separated catalyst was washed with hot ethanol, dried in an oven at 120 ºC for 2 h, and reused directly with fresh substrates under the optimized conditions. As shown in Figure 1, it was noticed that the recovered catalyst was recycled in subsequent runs without observation a significant decrease in activity even after ten runs.

**Table 1.** Screening the reaction parameters on the synthesis of 2-amino-5-oxo-5,6,7,8-tetrahydro-4*H*-chromene **5a**[a]

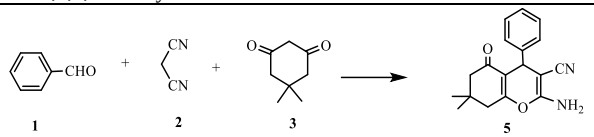


| Entry | Conditions | Catalyst (mol%) | Time (min) | Yield (%)[b] |
|---|---|---|---|---|
| 1 | $H_2O$ | $ZnFe_2O_4$ (5) | 10 | 78 |
| 2 | EtOH | $ZnFe_2O_4$ (5) | 10 | 82 |
| 3 | $CH_3CN$ | $ZnFe_2O_4$ (5) | 10 | 68 |
| 4 | EtOH/$H_2O$ (1:1) | $ZnFe_2O_4$ (5) | 10 | 87 |
| 5 | EtOH/$H_2O$ (2:1) | $ZnFe_2O_4$ (5) | 10 | 90 |
| 6 | EtOH/$H_2O$ (2:1) | $ZnFe_2O_4$ (8) | 10 | 91 |
| 7 | EtOH/$H_2O$ (2:1) | $ZnFe_2O_4$ (3) | 10 | 68 |
| 8 | EtOH/$H_2O$ (2:1) | No catalyst | 10 | 28 |
| 9 | EtOH/$H_2O$ (2:1) | $Fe_2O_3$ (5) | 10 | 61 |
| 10 | EtOH/$H_2O$ (2:1) | $Fe_3O_4$ (5) | 10 | 54 |
| 11 | EtOH/$H_2O$ (2:1) | $Ni_{0.7}Zn_{0.3}Fe_2O_4$ (5) | 10 | 71 |
| 12 | EtOH/$H_2O$ (2:1) | $Mn_{0.7}Zn_{0.3}Fe_2O_4$ (5) | 10 | 68 |

[a]Conditions: benzaldehyde (1 mmol), malononitrile (1 mmol), dimedone (1 mmol), rt. [b]Isolated Yield.

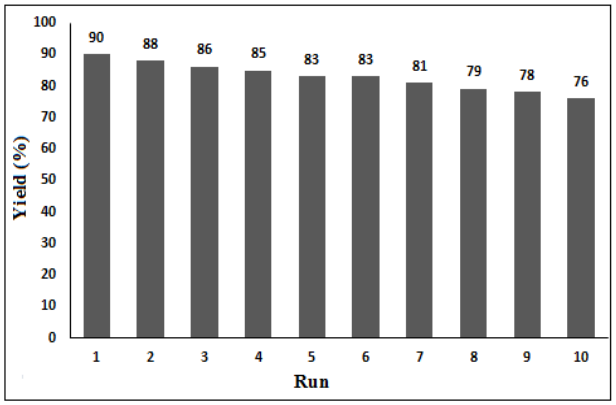


**Figure 1.** Recycling of $ZnFe_2O_4$ nanoparticles as the catalyst in the synthesis of 2-amino-5-oxo-5,6,7,8-tetrahydro-4*H*-chromene **5a**.

This achievement encouraged us to explore the generality of the magnetic $ZnFe_2O_4$ nanoparticles as a catalyst and extend the scope of the reaction to a series of variously substituted aromatic aldehydes under optimized conditions. All the reactions went to completion within a few minutes to furnish the respective 4*H*-chromenes **5a-j** in high to excellent yields (Table 2). Likewise, magnetic nano-$ZnFe_2O_4$ was found quite suitable to catalyze the synthesis of 4*H*-pyrano [2, 3-c] pyrazoles **6** in high yields from the one-pot reaction between the aromatic aldehydes, malononitrile and 3-methyl-1-phenyl-2-

**Table 2.** Synthesis of 4*H*-chromenes **5**, and 4*H*-pyrano[2,3-c]pyrazoles **6** under the catalytic effect of magnetic $ZnFe_2O_4$ nanoparticles[a]

| Entry | Ar | Product | Time (min) | Yield (%)[b] | Mp (°C) Found | Mp (°C) Ref |
|---|---|---|---|---|---|---|
| 1 | Ph | **5a** | 10 | 90 | 236-238 | 235-238[46] |
| 2 | 4-$FC_6H_4$ | **5b** | 10 | 92 | 193-195 | 191-193[47] |
| 3 | 4-$ClC_6H_4$ | **5c** | 10 | 91 | 214-216 | 215-216[45] |
| 4 | 3-$NO_2C_6H_4$ | **5d** | 10 | 88 | 213-215 | 213-217[51] |
| 5 | 4-$NO_2C_6H_4$ | **5e** | 12 | 85 | 181-182 | 181-184[50] |
| 6 | 4-$MeOC_6H_4$ | **5f** | 15 | 80 | 198-199 | 203-205[49] |
| 7 | 4-$MeC_6H_4$ | **5g** | 15 | 77 | 208-210 | 210-213[48] |
| 8 | 2-$ClC_6H_4$ | **5h** | 10 | 86 | 190-191 | 189-191[45] |
| 9 | 4-$OHC_6H_4$ | **5i** | 14 | 88 | 205-206 | 206-208[52] |
| 10 | 2-$NO_2C_6H_4$ | **5j** | 12 | 75 | 233-235 | 234-136[51] |
| 11 | Ph | **6a** | 14 | 87 | 169-170 | 169-171[53] |
| 12 | 4-$FC_6H_4$ | **6b** | 12 | 90 | 178-179 | 176-177[55] |
| 13 | 4-$ClC_6H_4$ | **6c** | 12 | 91 | 175-188 | 186-187[55] |
| 14 | 3-$ClC_6H_4$ | **6d** | 10 | 88 | 158-160 | 158-159[53] |
| 15 | 4-$BrC_6H_4$ | **6e** | 14 | 85 | 185-187 | 182-184[58] |
| 16 | 3-$NO_2C_6H_4$ | **6f** | 10 | 90 | 189-191 | 193-194[54] |
| 17 | 4-$NO_2C_6H_4$ | **6g** | 10 | 87 | 191-193 | 188-190[56] |
| 18 | 2,4-$Cl_2C_6H_3$ | **6h** | 14 | 84 | 185-187 | 185-186[57] |
| 19 | 3-EtO-4-$HOC_6H_3$ | **6i** | 15 | 83 | 172-173 | 170-171[57] |
| 20 | 1-Naphthyl | **6j** | 12 | 90 | 223-224 | 222-224[58] |

[a]Conditions: aromatic aldehyde (1 mmol), malononitrile (1 mmol), dimedone (1 mmol)/or 3-methyl-1-phenyl-2-pyrazolin-5-one (1 mmol), nano-$ZnFe_2O_4$ (5 mol%), EtOH/$H_2O$ (10:5 mL), rt.
[b]Isolated yield.

pyrazolin-5-one under the same optimized conditions. The experimental results are summarized in Table 2.

The superiority of the zinc ferrite $ZnFe_2O_4$ nanoparticles as a catalyst can be ascribed to the presence of $Zn^{2+}$ cations and its structural isotropy as well. The $Zn^{2+}$ cations present in the structure of $ZnFe_2O_4$ ferrite can significantly enhance the catalytic activity compared with $Fe^{2+}$ and $Fe^{3+}$ cations present in the structures of $Fe_2O_3$ and $Fe_3O_4$. As shown in Table 1, it is interesting to note that, the partial replacement of $Zn^{2+}$ cations with $Ni^{2+}$ or $Mn^{2+}$ cations in the structure of nano-$ZnFe_2O_4$ respectively in the forms of $Ni_{0.7}Zn_{0.3}Fe_2O_4$ and $Mn_{0.7}Zn_{0.3}Fe_2O_4$ brings about a reduction in the reaction yield. This fact suggests that the $Zn^{2+}$ cations perform stronger Lewis acid character in comparison with $Ni^{2+}$ and $Mn^{2+}$ cations. However, it is observed that the catalytic activities of the nano-ferrites $Ni_{0.7}Zn_{0.3}Fe_2O_4$ and $Mn_{0.7}Zn_{0.3}Fe_2O_4$ are relatively higher than the catalytic activities of the nano-ferrites $Fe_2O_3$ and $Fe_3O_4$ (Table 1). These results suggest that the $Ni^{2+}$ or $Mn^{2+}$ cations in turn have a more improving effect on the catalytic activity of these nano-magnetic oxides compared with the $Fe^{2+}$ and $Fe^{3+}$ cations. Moreover, the relatively higher catalytic ability exhibited by $Fe_2O_3$ containing only $Fe^{3+}$ cations in comparison with the $Fe_3O_4$ consisted of both the $Fe^{2+}$ and $Fe^{3+}$ cations, suggest that the catalytic power can be related to the structural isotropy and cation distribution.

Accordingly, all the sites in the structure of the nano-$Fe_2O_3$ are located in the same conditions. As a result, the ferrite $Fe_2O_3$ exists as an isotropic structure, whereas the ferrite $Fe_3O_4$ lacks such structural isotropy. As mentioned before, the $Zn^{2+}$ cations present in the magnetic $ZnFe_2O_4$ nano-catalyst occupy tetrahedral sites with similar conditions. This causes these octahedral sites to be isotropic that, in turn, enhances the catalytic power of the nano-ferrite $ZnFe_2O_4$ in the reaction. As the number of $Zn^{2+}$ cations is decreased with increasing the number of $Ni^{2+}$ or $Mn^{2+}$ cations in the structure of the $ZnFe_2O_4$, the $Ni^{2+}$ or $Mn^{2+}$ cations tend to occupy the octahedral sites with $Fe^{3+}$ cations being transferred to the tetrahedral sites. Such changes give rise to reduction of the structural isotropy and the catalytic powers of $Ni_{0.7}Zn_{0.3}Fe_2O_4$ and $Mn_{0.7}Zn_{0.3}Fe_2O_4$ nano-catalysts as well. A possible mechanism to support the formation of the 4*H*-chromenes **5** is depicted in Scheme 2. It is reasonable to assume that, in the initial step the aldehyde **1** undergoes condensation with malononitrile under the catalytic effect of $ZnFe_2O_4$ nanoparticles to generate the intermediate arylidenemalononitrile (**I**). Subsequent nucleophilic addition of enolizable dimedone **3** to the intermediate (**I**) leads to the formation of the second intermediate (**II**). The consecutive intramolecular cyclization of the intermediate (**II**) to the intermediate (**III**) occurs in the presence of magnetic nano-$ZnFe_2O_4$ catalyst followed by its rearrangement to furnish the expected 4*H*-chromenes **5**. A similar mechanism is expected to hold for the formation of 4*H*-pyrano [2, 3-c] pyrazoles **6**.

FT-IR spectra of $ZnFe_2O_4$ and recovered $ZnFe_2O_4$ are depicted in Figure 2. In FTIR spectrum of $ZnFe_2O_4$ confirmed absorption peak at 597 $cm^{-1}$, which is in association with 600-400 $cm^{-1}$, commonly observed for spinel ferrites. In this spectrum, intensive absorptions at

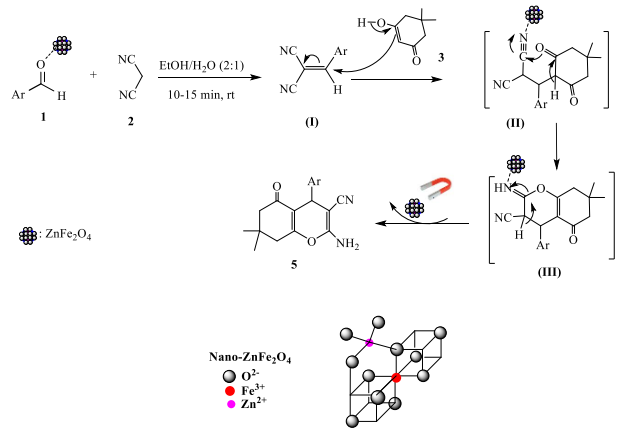


**Scheme 2.** The possible mechanism for synthesis of 4*H*-chromenes 5 in the presence of nano-$ZnFe_2O_4$ catalyst

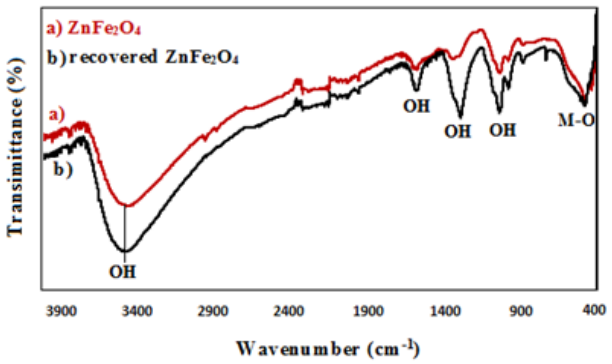


**Figure 2.** FT-IR spectra of a) $ZnFe_2O_4$ and b) recovered $ZnFe_2O_4$.

555 $cm^{-1}$ and 695 $cm^{-1}$ are related to vibration stretching of the metal-O bond in spinel ferrite. The absorption peak at 597 $cm^{-1}$ could be associated with Zn–O stretching in tetrahedral sites. A strong and broad characteristic absorptions peak at 3200-3500 $cm^{-1}$ is assigned to hydrogen-bonded stretch vibrations of O–H functional group. A strong and sharp characteristic absorptions peak at around 1650 $cm^{-1}$ is attributed to stretch bending vibrations of O–H functional group.[59-63] So, the presence of absorption peaks at 3389 and 1620 $cm^{-1}$ in the $ZnFe_2O_4$ spectrum represents H–O–H and OH vibration. These peaks confirm the presence of water molecules adsorbed on the surface due to the high specific surface area of the powders.[61]

The X-ray diffraction (XRD) spectrum of $ZnFe_2O_4$ synthesized by the LTSSR method is shown in Figure 3. The peaks of the as prepared solid indexed to the crystal plane of spinel Zn ferrite (111), (220), (311), (222), (400), (422), (511), (440), (620), and (533), respectively. The X-ray pattern of the as-prepared ferrite displays sharp and well-resolved diffraction peaks with the good crystallinity of the as-prepared specimen. No additional peak of the second phase was observed in the XRD pattern, showing that the as prepared ferrite consisted of single spinel $ZnFe_2O_4$ phase. Also, the peaks were indexed by comparing the interplanar distance with JCPDS data (JCPDS card no. 10-325, 22-1086), corresponding to $Ni_{0.7}Zn_{0.3}Fe_2O_4$ ferrite and $Mn_{0.7}Zn_{0.3}Fe_2O_4$ ferrite respectively (Figure 4a,b). SEM images (Figure 5) indicate a particulate morphology with an average particle size of 10 nm for the synthesized product.

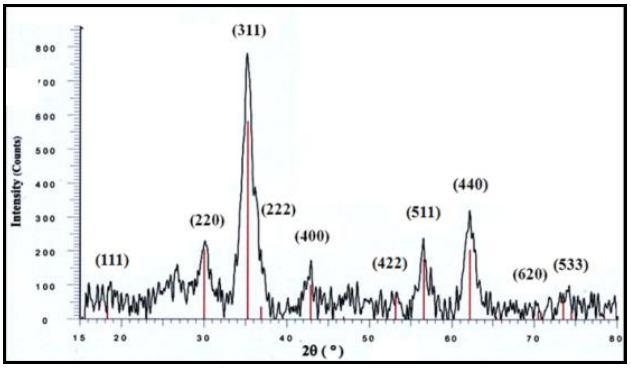


**Figure 3.** XRD pattern of Nano-Ferrite $ZnFe_2O_4$.

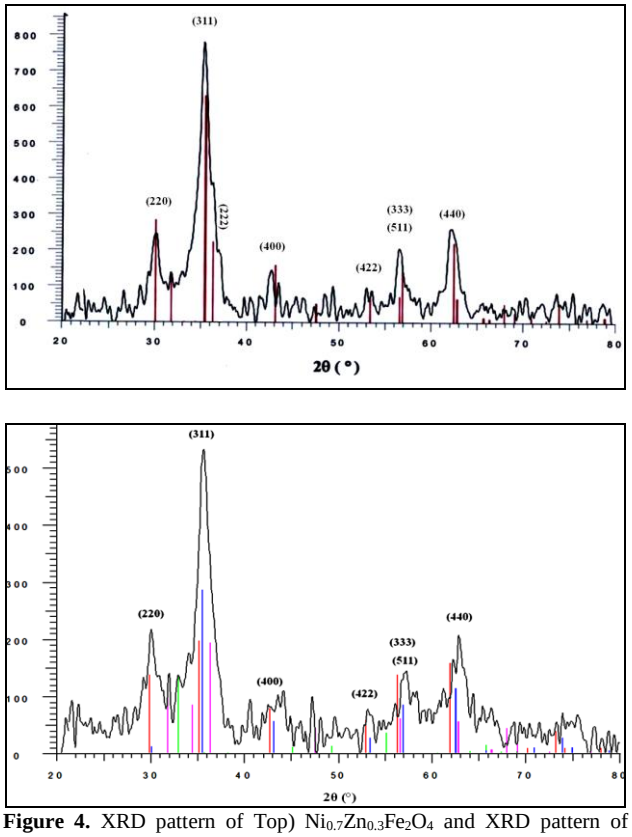


**Figure 4.** XRD pattern of Top) $Ni_{0.7}Zn_{0.3}Fe_2O_4$ and XRD pattern of Bottom) $Mn_{0.7}Zn_{0.3}Fe_2O_4$.

The TEM image recorded for the $ZnFe_2O_4$ is given in Figure 6. The particles are well separated. The morphology of particles is faceted in nature suggested good crystalline growth and the mean size is about 10–15 nm.

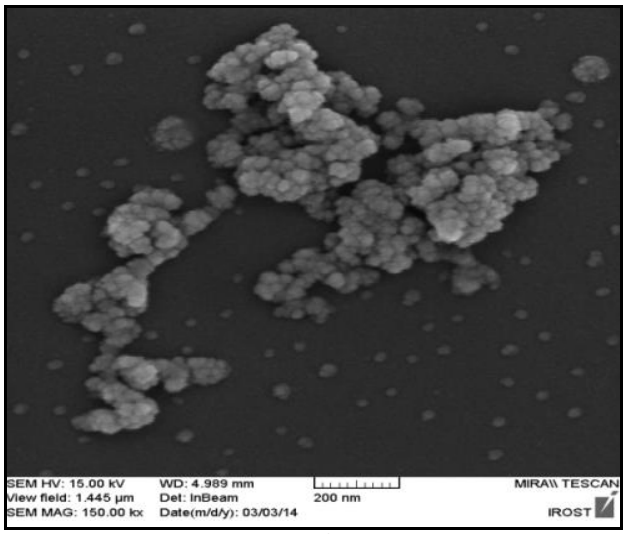


**Figure 5**. The SEM micrographs of Nano-Ferrite $ZnFe_2O_4$.

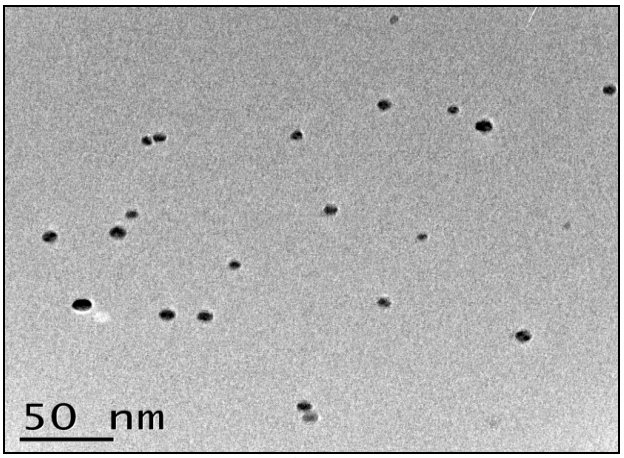


**Figure 6.** The HR-TEM images of Nano-Ferrite $ZnFe_2O_4$.

The compositional analysis has been characterized using EDAX in order to confirm the elements present in $ZnFe_2O_4$ as catalyst (Figure. 7). The peaks of Fe, Zn and, O are observed with the atomic percentage of 39.43, 20.0 and 40.56 %. No other traced amount of impurity element was observed from the synthesized product.

Figure 8 shows the magnetic properties of the catalyst $ZnFe_2O_4$ that was investigated at room temperature using a vibrating sample magnetometer (VSM). Based on magnetization curves, the magnetization is saturated up to 8 emu/g at an applied field of 9000 Oe, with an almost insignificant coercively. Thus, it could simply be recovered in a short time (<60 s) by fixing a magnet near to the reaction vessel.

## 2. EXPERIMENTL

Chemicals were purchased from Fluka and Merck Chemical Companies and used without purification. $^1H$ NMR and $^{13}C$ NMR spectra were measured for samples in DMSO-$d_6$ using a Bruker Avance 300 MHz instrument (DRX). Melting points were determined with a SMPI apparatus. The products were characterized by X-ray powder diffraction (XRD) on Holland Philips X-pert diffractometer (Cu Kα = 1.5418 Å). The FT-IR spectra were recorded on a Thermo Scientific NICOLET IR100 FT-IR Spectrometer. The pellets made with KBr and the catalysts were prepared before the analyses. Morphology and particle dispersion were investigated by scanning electron microscopy (SEM) (Philips XL30). Transmission electron microscopy (TEM) images were performed on an EM10C (Zeiss) transmission electron microscope at an accelerating voltage of 80 kV. The corresponding Energy-dispersive X-ray (EDAX) spectrum was obtained on a Holland Philips XL30 microscope instrument. Magnetic measurement of materials was carried out with a vibrating sample magnetometer VSM (4 inches, Daghigh Meghnatis Kashan Co., Kashan, Iran) at room temperature.

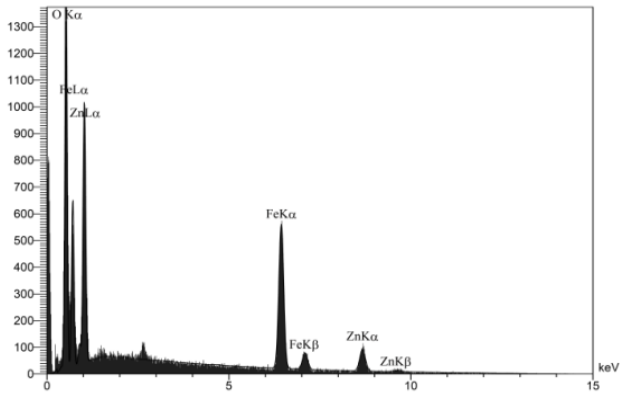


**Figure 7.** Energy dispersive X-ray (EDX) analysis of $ZnFe_2O_4$.

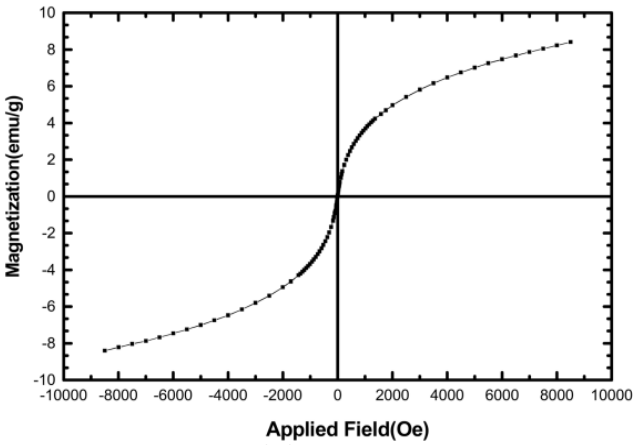


**Figure 8** The VSM analysis of of Nano-Ferrite $ZnFe_2O_4$.

### Preparation of catalyst

The magnetic $ZnFe_2O_4$, $Ni_{0.7}Zn_{0.3}Fe_2O_4$, $Mn_{0.7}Zn_{0.3}Fe_2O_4$ nanoparticles with average grain sizes ranging from 10 to 60 nm and behaving as superparamagnetic at room temperature have been produced using a low-temperature solid-state reaction (LTSSR) method.[64,65] In a typical experiment for the synthesis of these nanoparticles, powders of $ZnCl_2$, $MnCl_2.6H_2O$ or, $NiCl_2.6H_2O$ were mixed with $FeCl_3.6H_2O$ and NaOH in their appropriate stoichiometric ratios (1:2:8) and (1:1:2:8) respectively. In each case, the mixture was milled at room

temperature for 30 min in an aqueous medium. Finally, the resulting mixture was repeatedly washed with double-distilled water and acetone, and the nanoparticles were calcined in a furnace set at 800 ºC (LTS80) for 3 h. In this method, instead of co-precipitation a chemical reaction takes place. The magnetic $Fe_3O_4$ nanoparticles were synthesized by the co-precipitation method and transformed into maghemite ($\gamma$-$Fe_2O_3$) by air oxidation at 200 ºC as reported first by Massart.[66] As described in the literature,[67-69] powders of $FeCl_2$, $FeCl_3$ and, NaOH were mixed in the stoichiometric ratio (1:2:8) and dissolved in distilled water. Then, an aqueous NaOH solution was added and the resulting iron solutions were vigorously stirred until the mixing was completed. As a result, the color of the solutions turned into black indicating the nucleation of the $Fe_3O_4$ nanoparticles. The resulting precipitate was separated by magnetic decantation and washed several times consecutively with distilled water and ethanol. The magnetic nanoparticles were then dried in an oven at 60 ºC. To obtain the maghemite ($\gamma$-$Fe_2O_3$), a part of the dried magnetite nanoparticles was heated at 200 ºC for 3 hrs and collected as red-brown nanoparticles.

**General Procedure for the Synthesis of 4*H*-Chromenes 5 and 4*H*-Pyrano[2,3-c]pyrazoles 6:**

To a mixture of the appropriate aromatic aldehyde (1 mmol), malononitrile (1 mmol), and nano-catalyst $ZnFe_2O_4$ (5 mol %) in EtOH/$H_2O$ (10:5 mL) was added dimedone (1 mmol) or 3-methyl-1-phenyl-2-pyrazoline-5-one (1 mmol). The resulting mixture was stirred at room temperature for an appropriate time (Table 2). After the completion of the reaction as monitored by TLC analysis, hot absolute ethanol (5 mL) was added to the resulting mixture. The magnetic nanoparticles were separated by absorbing on the magnetic stirring bar. Then, the remaining mixture was evaporated under reduced pressure to leave the crude product which was purified by crystallization from absolute ethanol. The known products **5a-j** and **6a-j** were characterized on the basis of their physical and spectral (IR, $^1$H NMR, $^{13}$C NMR) data which were in accord with the reported data.[33-38]

## 4. CONCLUSIONS

In summary, the spinel ferrite $ZnFe_2O_4$ nanoparticles were explored as an effective and reusable catalyst for the synthesis of 2-amino-5-oxo-5,6,7,8-tetrahydro-4*H*-chromenes and, 1, 4-dihydropyrano [2, 3-c] pyrazol-5-yl cyanides in EtOH/$H_2O$ at room temperature. It was found that the catalytic power of various spinel ferrites examined in the titled reactions is related to the structural isotropy, cation distribution and, the Lewis acid character of the cations embedded in the structures of these ferrites. Accordingly, the $Zn^{2+}$ cations in the structure of the nano-zinc ferrite $ZnFe_2O_4$ exhibited the highest structural isotropy and Lewis acid strength leading to the better catalytic performance by magnetic $ZnFe_2O_4$ nanoparticles.

## CONFLICTS OF INTEREST

The authors have declared that there is no conflict of interest.

## ACKNOWLEDGMENTS

The authors wish to thank the research council of Kosar University, Bojnoord for financial support to carry out this research.

## AUTHOR INFORMATION

**Corresponding Author**

Razieh Nejat: Email: organochem.nejat@yahoo.com, *ORCID*: 0000-0001-8742-2342

## REFERENCES

1. D. Astruc, F. Lu, J. R. Aranzaes, *Angew. Chem. Int. Ed.* **2005**, *44*, 7852-7872.
2. M. T. Reetz, M. Maase, *Adv. Mater.* **1999**, *11*, 773-777.
3. B. M. Choudary, M. L. Kantam, K. V. S. Ranganath, K. Mahender, B. Sreedhar, *J. Am. Chem. Soc.* **2004**, *126*, 3396-3397.
4. B. M. Choudary, R. S. Mulukutla, K. J. Klabunde, *J. Am. Chem. Soc.* **2003**, *125*, 2020-2021.
5. J. A. Melero, R. V. Grieken, G. Morales, *Chem. Rev.* **2006**, *106*, 3790-3812.
6. S. Morent, S. Vasseur, F. Grasset, E. Duguet, *J. Mater. Chem.* **2004**, *14*, 2161-2175.
7. V. Polshettiwar, B. Baruwati, R. S. Varma, *Green Chem.* **2009**, *11*, 127-131.
8. A. J. Amali, R. K. Rana, *Green Chem.* **2009**, *11*, 1781-1795.
9. B. Baruwati, V. Polshettiwar, R. S. Varma, *Tetrahedron Lett.* **2009**, *50*, 1215-1218.
10. V. Polshettiwar, R. S. Varma, Org. Biomol. Chem. **2009**, 7, 37-40.
11. S. Shylesh, J. Schweizer, S. Demeshko, V. Schunemann, S. Ernst, W. R. Thiela, *Adv. Synth. Catal.* **2009**, *351*, 1789-1795.
12. A. G. Hu, G. T. Yee, W. B. Lin, *J. Am. Chem. Soc.* **2005**, *127*, 12486-12487.
13. M. Chahkandi, A. Amiri, *Inorg. Chem. Res.* **2019**, *2*, 50-64.
14. G. Mohammadnezhada, F. Ariaeinezhada, F. Steiniger, *Inorg. Chem. Res.* **2019**, *2*, 129-136.15.
15. M. Ahmadi, M. Bahadori, V. Mirkhani, M. Moghadam, S. Tangestaninejad, I. Mohammadpoor-Baltork, *Inorg. Chem. Res.* **2020**, *4*, 51-65.
16. E. Rafiee, S. Kazemi, S. Eavani, *Inorg. Chem. Res.* **2020**, *4*, 1-9.
17. F. Keshavarzipour, H. Tavakol, *Appl. Organometal Chem.* **2016**, *31*, 1-8.
18. H. Tavakol, F. Keshavarzipour, *Appl. Organometal Chem.* **2017**, *31*, 1-9.
19. R. B. N. Baig, R. S. Varma, *Chem. Commun.* **2012**, *48*, 2582-2584.
20. A. Maleki, Z. Varzi, F. Hassanzadeh-Afruzi, *Polyhedron*, **2019**, *171*, 193-202.

21. M. Taqi Jafari-Chermahini, H. Tavakol, *Chem. Select.* **2019**, *4*, 1895-1902.
22. B. Cullity, Elements of X-Ray Diffraction, Addison Wesley Inc, **1977**.
23. K. Sreekumar, T. Raja, B. Kiran, S. Sugunan, B. Rao, *Appl. Catal. A.* **1999**, *182*, 327-336.
24. I. B. Bersuker, Electronic Structure and Properties of Transition Metal Compounds: Introduction to the Theory, New York, Wiley, **1996**.
25. R. Burns, Mineralogical Applications of Crystal Field Theory, Cambridge: Cambridge University Press, **1993**.
26. R. J. Borg, G. J. Dienes, Physical Chemistry of Solids (Academic: San Diego, CA), **1992**.
27. A. Goldman, Modem Ferrite Technology, 2nd ed., P. A. Pittsburgh, USA, **1987**.
28. J. Zhu, K. J. Tseng, *IEEE Trans. Magn.* **2004**, *40*, 3339-3345.
29. A. Dömling, I. Ugi, *Angew. Chem. Int. Ed.* **2000**, *39*, 3168-3210.
30. B. Ganem, *Acc. Chem. Res.* **2009**, *42*, 463-472.
31. S. Brase, C. Gil, K. Knepper, *Bioorg. Med. Chem.* **2002**, *10*, 2415-2437.
32. L. L. Andreani, E. Lapi, *Bull. Chim. Farm.* **1960**, *99*, 583-586.
33. S. Gao, C. H. Tsai, C. Tseng, C. F. Yao, *Tetrahedron*, **2008**, *64*, 9143-9149.
34. D. Kumar, V. B. Reddy, S. Sharad, U. Dube, S. Kapur, *Eur. J. Med. Chem.* **2009**, *44*, 3805.
35. D. Shi, J. Mou, Q. Zhuang, L. Niu, N. Wu, X. Wang, *Synth. Commun.* **2004**, *34*, 4557-4263.
36. T. S. Jin, A. Q. Wang, Z. L. Cheng, J. S. Zhang, T. Li, *Synth. Commun.* **2005**, *35*, 137-143.
37. S. B. Guo, S. X. Wang, J. T. Li, *Synth.Commun.* **2007**, *37*, 2111-2120.
38. A. Azarifar, R. Nejat-Yami, D. Azarifar, *J. Iran. Chem. Soc.* **2013**, *10*, 439-446.
39. T. S. Jin, R. Q. Zhao, T. S. Li, *Arkivoc*, **2006**, *11*, 176-182.
40. H. Sheibani, M. Babaie, *Synth. Commun.* **2010**, *40*, 257-265.
41. D. Azarifar, R. Nejat-Yami, M. A. Zolfigol, *J. Heterocycl. Chem.* **2013**, *50*, 1386-1390.
42. M. A. Zolfigol, T. Azadbakht, V. Khakyzadeh, R. Nejat Yami, D. M. Perrin, *RSC Adv.* **2014**, *4*, 40036-40042.
43. D. Azarifar, R. Nejat-Yami, Z. Akrami, F. Sameri, S. Samadi, *Lett. Org. Chem.* **2012**, *9*, 128-132.
44. M. Balali, M. Bagherzadeh, R. Nejat, H. Keypour, *Inorg. Chem. Res.* **2021**, *5*, 82-93.
45. S. Khaksar, A. Rouhollahpour, S. M. Talesh, *J. Fluorine Chem.* **2012**, *141*, 11-15.
46. D. Azarifar, Y. Abbasi, O. Badalkhani, *J. Adv. Chem.* **2014**, *10*, 3197-3202.
47. D. Fang, H. B. Zhang, Z. L. Liu, *J. Heterocycl. Chem.* **2010**, *47*, 63-67.
48. D. Azarifar, S. M. Khatami, R. Nejat-Yami, *J. Chem. Sci.* **2014**, *126*, 95-101.
49. J. C. Xu, W. M. Li, Z. Zheng, Y. F. Lai, P. F. Zhang, *Tetrahedron*. **2011**, *67*, 9582-9587.
50. L. Q. Yu, F. Liu, Q. D. You, *Org. Prep. Proced. Int.* **2009**, *41*, 77-82.
51. S. Balalaie, M. Bararjanian, M. Sheikh-Ahmadi, S. Hekmat, P. Salehi, *Synth. Commun.* **2007**, *37*, 1097-1108.
52. S. Sarrafi, E. Mehrasbi, A. Vahid, M. Tajbakhsh, *Chin. J. Catal.* **2012**, *33*, 1486-1494.
53. T. S. Jin, A. Q. Wang, Z. L. Cheng, J. S. Zhang, T. S. Li, *Synth. Commun.* **2005**, *35*, 137-143.
54. S. B. Guo, S. X. Wang, J. T. Li, *Synth. Commun.* **2007**, *37*, 2111-2120.
55. L. G. Sharanina, V. K. Promonenkov, V. P. Marshtupa, A. V. Pashchenko, V. V. Puzanova, Yu. A. Sharanin, N. A. Klyuev, L. F. Gusev, A. P. Gnatusina, *Chem. Het. Comp.* **1982**, *18*, 1-7.
56. A. Saha, S. Payra, S. Banerjee, *Green Chem.* **2015**, *17*, 2859-2866.
57. M. Farahi, B. Karami, I. Sedighimehr, H. Mohamadi Tanuraghaj, *Chin. Chem. Lett.* **2014**, *25*, 1580-1582.
58. A. Saha, S. Payra, S. Banerjee, *Green Chem.* **2015**, *17*, 2859-2866.
59. R. M. Silverstein, F. X. Webster, D. J. Kiemle, D. L. Bryce, Spectrometric Identification of Organic Compounds, Wiley, New York, **2014**.
60. S. A. Hosseini, V. Majidi, A. R. Abbasian, *J. Sulfur. Chem.* **2018**, *39*, 119-129.
61. J. Kurian, M. J. Mathew, *J. Magn. Magn. Mater.* **2018**, *451*, 121-130.
62. M. Araghi, M. Ghahari, M. S. Afarani, *J. Environ. Chem. Eng.* **2017**, *5*, 1780-1790.
63. M. M. Naiini, M. Ghahari, M. S. Afarani, *Part Sci. Technol.* **2015**, *33*, 456-462.
64. Gh. R. Amiri, M. H. Yousefi, M. R. Abolhassani, S. Manouchehri, M. H. Keshavarz, S. Fatahian, *J. Magn. Magn. Mater.* **2011**, *323*, 730-734.
65. F. Li, H. Wang, L. Wang, J. Wang, *J. Magn. Magn. Mater.* **2007**, *309*, 295-299.
66. R. Massart, *IEEE Trans. Magn.* **1981**, *17*, 1247-1248.
67. A. Predescu, *Bulletin of the Polytechnic Institute of Jassy, LVI (LX)*, **2010**, *2*, 95-102.
68. M. A. Legodi, D. de Waal, *Dyes Pigments*. **2007**, *74*, 161-168.
69. D. L. A. Faria, S. V. Silva, M. T. Oliveira, *J. Raman. Spectrosc.* **1997**, *28*, 873-878.